



CHORUS

This is the accepted manuscript made available via CHORUS. The article has been published as:

Correlated random hopping disorder in graphene at high magnetic fields: Landau level broadening and localization properties

A. L. C. Pereira, C. H. Lewenkopf, and E. R. Mucciolo

Phys. Rev. B **84**, 165406 — Published 4 October 2011

DOI: [10.1103/PhysRevB.84.165406](https://doi.org/10.1103/PhysRevB.84.165406)

Correlated random hopping disorder in graphene at high magnetic fields: Landau level broadening and localization properties

A. L. C. Pereira,¹ C. H. Lewenkopf,² and E. R. Mucciolo³

¹*Faculdade de Ciências Aplicadas, Universidade Estadual de Campinas, 13484-350 Limeira SP, Brazil*

²*Instituto de Física, Universidade Federal Fluminense, 24210-346 Niterói RJ, Brazil*

³*Department of Physics, University of Central Florida, Orlando, FL 32816-2385, USA*

(Dated: September 12, 2011)

We study the density of states and localization properties of the lowest Landau levels of graphene at high magnetic fields. We focus on the effects caused by correlated long-range hopping disorder, which, in exfoliated graphene, is induced by static ripples. We find that the broadening of the lowest Landau level shrinks exponentially with increasing disorder correlation length. At the same time, the broadening grows linearly with magnetic field and with disorder amplitudes. The lowest Landau level peak shows a robust splitting, whose origin we identify as the breaking of the sublattice (valley) degeneracy.

PACS numbers: 73.43.-f, 73.63.-b, 71.70.Di

I. INTRODUCTION

The observation of the anomalous quantum Hall effect^{1,2} is one of the most striking and robust manifestations of the underlying massless Dirac fermions in graphene near half filling. The energy scales in graphene are such that the quantization of the Hall plateaus can be observed even at room temperature at sufficiently high magnetic fields.³ The energetics in graphene also favors a direct experimental access to the low-lying Landau levels by infrared spectroscopy⁴⁻⁶ and by scanning tunneling spectroscopy,^{7,8} something hardly possible in conventional semiconductors.

Further information about the nature of the lowest Landau levels in graphene has been recently obtained in thermal activation experiments,⁹⁻¹³ showing that the zeroth Landau level ($n = 0$) is much sharper than the first and higher Landau levels. These observations are the main motivation of the theoretical study presented in this paper.

Disorder is key to understand the electronic transport properties in graphene,¹⁴⁻¹⁷ particularly in the quantum Hall regime, where the conductivity plateaus are conventionally explained by delocalized states surrounded by localized ones. However, the mechanisms that lead to localization in QHE in graphene are still not clear.¹⁸ Currently, there is still some debate on the most relevant disorder mechanisms for transport in graphene.¹⁵ Among those, ripple disorder is believed to play an important role. Static ripples give rise to random correlated hopping disorder,^{19,20} which is the disorder mechanism analyzed in this paper.

The shape and width of the lowest Landau levels (LLs) in graphene have been investigated in several theoretical studies.²¹⁻²⁹ The broadening of the LLs differs among disorder models. In particular, the inclusion of a finite correlation length on the hopping (off-diagonal) disorder model was recently reported to induce an anomalously sharp $n = 0$ LL compared to higher levels.^{25,26} It was

found that the width of the zeroth LL (Γ_0) shrinks to zero as soon as the hopping correlation length λ exceeds the lattice parameter a , in line with analytical studies of the effects of long-range chiral disorder.³⁰

Regarding the localization properties of the lowest LL, numerical simulations using uncorrelated hopping disorder^{21,24} and white-noise random magnetic flux disorder^{31,32} observe an interesting distinct qualitative feature in the quantum Hall spectrum of graphene, namely, a splitting. It was found that, in such chiral disorder models, the lowest LL splits into two Gaussian shaped peaks, even in the absence of both a Zeeman term and electron-electron interactions. The splitting energy ΔE is linearly proportional to the disorder strength and scales with the square root of the applied perpendicular magnetic field.^{24,31} A similar square root magnetic field dependence of the splitting of the $n = 0$ Landau level has been experimentally observed in Ref. 9.

In this paper, instead of the white-noise random hopping (or magnetic flux) model, we address the more realistic correlated random hopping disorder model.^{25,26} We present a systematic study of the shape of the lowest LLs and their localization properties as a function of the hopping disorder correlation length, as well as of other relevant parameters of the system, such as disorder amplitude and magnetic field. We find that Γ_0 decays exponentially with the correlation length, never fully vanishing for any finite λ . More importantly, we observe that the ratio Γ_1/Γ_0 depends only on the disorder correlation length, showing no significant variation neither with the disorder strength, nor with the magnitude of the applied magnetic field B , provided the system is in the quantum Hall regime. In addition, we study the splitting of the $n = 0$ LL, which is inferred from the analysis of the participation ratio. We show that this splitting shrinks with increasing values of λ , but is still present even for correlation lengths for which the $n = 0$ LL width becomes very small.

The paper is organized as follows. In Sec. II, we present the model used in our numerical simulations.

The analytical framework for the interpretation of our results is discussed in Sec. III. Next, we analyze the spectral, Sec. IV, and localization properties, Sec. V, of the model. We conclude summarizing our results and discussing their relevance to the interpretation of experiments on the quantum Hall effect in graphene in Sec. VI.

II. MODEL DESCRIPTION

Graphene is a monolayer honeycomb lattice of carbon atoms with a lattice constant $a = 2.46 \text{ \AA}$. Its primitive unit cell contains a pair of atoms that form two triangular sublattices, denoted by A and B . The tight-binding Hamiltonian model for a graphene monolayer reads

$$H = \sum_{\langle ij \rangle} \left(t_{ij} e^{i\phi_{ij}} c_i^\dagger c_j + \text{H.c.} \right), \quad (1)$$

where the sum runs over nearest-neighbor sites. The external magnetic field B , perpendicular to the graphene sheet, is included by Peierls' substitution, namely, $\phi_{ij} = 2\pi(e/h) \int_{r_j}^{r_i} \mathbf{A} \cdot d\mathbf{l}$. In the Landau gauge, $\mathbf{A} = (0, Bx)$ and considering a brick wall lattice, which is topologically equivalent to the hexagonal lattice,³³ one has $\phi_{ij} = 0$ along the x direction and $\phi_{ij} = \pm\pi(x/a)\Phi/\Phi_0$ along the $\mp y$ direction, with $\Phi/\Phi_0 = Ba^2\sqrt{3}e/(2h)$ per unit cell.

The random hopping disorder is implemented by randomly choosing the hopping parameters t_{ij} from a uniform distribution of width W around the average value $t = 2.7 \text{ eV}$. In addition, we impose here a spatial correlation to the hoppings following a Gaussian profile of width λ . Figure 1 illustrates typical realizations of the disordered hopping parameter t_{ij} for two different correlation lengths ($\lambda = 2a, 4a$). The color scale refers to the hopping amplitude at the middle point between the two nearest-neighbor sites i and j . As expected, Fig. 1 shows smoother (less abrupt) variations of the hopping values with increasing correlation length.

We consider graphene lattices of $M \times N$ carbon atoms (M zigzag chains, each containing N atoms) with periodic boundary conditions. The linear sizes of the lattices are

$$L_x = (M-1)\frac{\sqrt{3}}{2}a, \quad L_y = (N-1)\frac{a}{2}. \quad (2)$$

Most of the numerical results shown in this paper are calculated for lattices of $M \times N = 100 \times 90$ atoms, corresponding to a size $L_x \times L_y = 21.1 \text{ nm} \times 10.9 \text{ nm}$, the same lattice dimensions shown in Fig. 1.

III. DIRAC HAMILTONIAN: ANALYTICAL RESULTS

Near half filling, the low-energy properties of the tight-binding Hamiltonian in Eq. (1) are described by noninteracting massless Dirac fermions in a uniform perpendicular magnetic field, with an effective Hamiltonian given

by^{34,35}

$$H_0 = v_F \begin{pmatrix} 0 & \pi_x - i\pi_y & 0 & 0 \\ \pi_x + i\pi_y & 0 & 0 & 0 \\ 0 & 0 & 0 & \pi_x + i\pi_y \\ 0 & 0 & \pi_x - i\pi_y & 0 \end{pmatrix}, \quad (3)$$

where $\hbar v_F = \sqrt{3}at/2$ is the Fermi velocity, $\boldsymbol{\pi} = \mathbf{p} + e\mathbf{A}/c$, and \mathbf{p} stands for the electron momentum operator. The Hamiltonian (3) operates on a four-components wave function $(\Psi_A^K, \Psi_B^K, \Psi_A^{K'}, \Psi_B^{K'})$, where Ψ_A^K and Ψ_B^K represent the envelope functions at A and B sites for the K point and $\Psi_A^{K'}$ and $\Psi_B^{K'}$ for K' , respectively. In this paper we do not consider explicitly the electron spin degree of freedom and all states are assumed spin degenerate.

The eigenstates of the Hamiltonian (3) are labeled by (j, n, k) , with the valley index $j = K, K'$, the Landau level index $n = 0, \pm 1, \dots$, and the wave vector k along y direction.³⁴ The eigenenergy depends solely on n as $\varepsilon_n = \hbar\omega_B \text{sgn}(n)\sqrt{|n|}$, where $\hbar\omega_B = \sqrt{2}\gamma/\ell_B$ with the magnetic length given by $\ell_B = \sqrt{\hbar/eB}$. For $\Phi/\Phi_0 < 0.05$, which implies $\ell_B/a \gg 1$, lattice size effects have a negligible influence on the graphene LLs in this model.

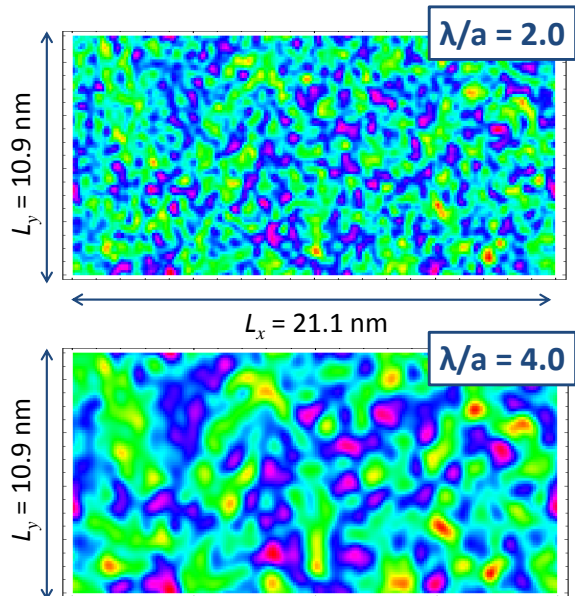


FIG. 1: (Color online) Typical spatial “landscapes” of the fluctuation in the hopping matrix elements $\delta t_{ij}/W = (t_{ij} - t)/W$ for two different correlation lengths ($\lambda = 2a, 4a$). The color scale represents the magnitude of $\delta t_{ij}/W$. The lattices shown above have $M \times N = 100 \times 90$ atoms, which corresponds to lateral dimensions $L_x \times L_y = 21.1 \text{ nm} \times 10.9 \text{ nm}$.

The eigenfunctions are written as

$$\Psi_{nk}^K = \frac{C_n}{\sqrt{L}} \exp(iky) \begin{pmatrix} \text{sgn}(n)(-i)\phi_{|n|-1,k} \\ \phi_{|n|,k} \\ 0 \\ 0 \end{pmatrix}, \quad (4)$$

$$\Psi_{nk}^{K'} = \frac{C_n}{\sqrt{L}} \exp(iky) \begin{pmatrix} 0 \\ 0 \\ \phi_{|n|,k} \\ \text{sgn}(n)(-i)\phi_{|n|-1,k} \end{pmatrix}. \quad (5)$$

Here $C_n = 1$ for $n = 0$, $C_n = 1/\sqrt{2}$ for $n \neq 0$, and

$$\phi_{n,k}(x) = (2^n n! \sqrt{\pi} \ell_B)^{-1/2} e^{-z^2/2} H_n(z), \quad (6)$$

with $z = (x - k\ell_B^2)/\ell_B$ and $H_n(z)$ denoting Hermite polynomials.

It was realized early²¹ that the level with $n = 0$ is special since its amplitude is non-zero only in one of the sublattices, namely, at B sites for K and A sites for K' . Consequently, while a random on-site disorder potential gives only intravalley mixing within either the K and K' valleys, random hopping causes intervalley mixing. (Notice that this is quite the opposite of what occurs at zero magnetic field when diagonal disorder is present.) The wave function in LLs with $n \neq 0$ has nonzero amplitudes on both A and B sites, so that intervalley mixing is always possible.

In this study, we consider hopping disorder caused by randomness in the hopping integral connecting neighboring A and B sites. This disorder can be long ranged, when caused by static ripples, or short ranged, when originated by scatterers located at points in-between neighboring sites.

Assuming that t shifts to $t + \delta t$ between neighboring sites \mathbf{R}_A and \mathbf{R}_B , hopping disorder gives rise to a short-range potential given by²¹

$$U(\mathbf{r}) = \begin{pmatrix} 0 & z_A^* z_B & 0 & z_A^* z_B' \\ z_B^* z_A & 0 & z_B^* z_A' & 0 \\ 0 & z_A'^* z_B & 0 & z_A'^* z_B' \\ z_B'^* z_A & 0 & z_B'^* z_A' & 0 \end{pmatrix} u_h \delta(\mathbf{r} - \mathbf{R}_i), \quad (7)$$

with $u_h = (\sqrt{3}a^2/2)\delta t$, $z_X = e^{i\mathbf{K}\cdot\mathbf{R}_X}$, and $z_X' = e^{i\mathbf{K}'\cdot\mathbf{R}_X}$ for $X = A$ and B . For a hopping disorder concentration n_h , the self-consistent Born approximation estimates the Landau level broadening as $\Gamma_{\text{short}} = (2n_h)^{1/2} u_h / (\pi \ell_B)$, independent of Landau level index. Numerical simulations²⁴ exhibit the same scaling of Γ_{short} with \sqrt{B} , but show that Γ_{short} increases with the index n .

Alternatively, when the randomness in the hopping integrals shows long-range correlations, the disorder Hamiltonian can be formulated in terms of an effective random magnetic field.^{20,36} In this case, one assumes that lattice deformations cause a smooth shift in the hopping integrals between the site j and its three nearest neighbors i . At low energies, this effect can be incorporated into Dirac

Hamiltonian by introducing an effective vector potential that reads

$$A_{\pm}^{\text{eff}}(\mathbf{r}_j) = \frac{c}{e} \sum_{i=1}^3 \delta t_i(\mathbf{r}_j) e^{\pm i\mathbf{q}_0 \cdot \hat{\mathbf{e}}_i}. \quad (8)$$

Here, $A_{\pm}^{\text{eff}} = A_x^{\text{eff}} \mp iA_y^{\text{eff}}$, \mathbf{e}_i are vector connecting a lattice site to its neighbors, and $\mathbf{q} \approx \pm\mathbf{q}_0$, where $\mathbf{q}_0 = 4\pi/(3\sqrt{3}a)\mathbf{e}_y$ with the Cartesian coordinate x running along the armchair direction. The subscript $+$ ($-$) corresponds to the K (K') valley. Random hopping is accounted for by adding the effective vector potential \mathbf{A}^{eff} to the momentum operator $\boldsymbol{\pi}$ appearing in Eq. (3), namely,³⁶

$$H_{\pm} = v_F \begin{pmatrix} 0 & \pi_x - i\pi_y + \frac{e}{c} A_{\pm}^{\text{eff}} \\ \pi_x + i\pi_y + \frac{e}{c} A_{\pm}^{\text{eff}*} & 0 \end{pmatrix}. \quad (9)$$

Notice that the effect of A_{\pm}^{eff} is to locally shift the Dirac cones K and K' in opposite directions and there is no valley mixing. The structure of H_{\pm} immediately reveals that the $n = 0$ states are unique: Since $\langle \Psi_{0k}^K | H - H_0 | \Psi_{0k'}^{K'} \rangle = 0$, in lowest order, long-range hopping disorder does not affect the $n = 0$ states.

Unfortunately, there is no such simple picture for treating the crossover regime between short- and long-range hopping disorder. In the following, we interpret the results of our numerical simulations by invoking the pure long-range description provided by Eq. (9), what is known about short-range hopping disorder, and by building a plausible interpolation between these two limits.

IV. SPECTRAL PROPERTIES

In this Section, we analyze the spectral properties of graphene obtained from the tight-binding model with correlated random hopping presented in Sec. II. We will focus our attention on the width of the disorder-broadened Landau levels and its dependence on the disorder correlation length λ , on the disorder amplitude W , on the magnetic flux Φ , and on the LL index n .

Figure 2a shows the density of states (DOS) corresponding to the four lowest LLs ($n = 0, 1, 2$, and 3) broadened by a correlated random hopping disorder of amplitude $W/t = 0.3$ for different correlation lengths, namely, $\lambda/a = 1, 2$, and 4 . Since particle-hole symmetry is preserved by the nearest-neighbor hopping disorder model, we only show the $n \geq 0$ LLs. The magnetic flux considered is $\Phi/\Phi_0 = 0.02$. The results typically correspond to averages over 600 disorder realizations.

Figures 2b and 2c are zooms of the DOS around the $n=0$ and the $n=1$ LLs, respectively, indicating that the broadening shrinks for increasing values of λ . An inspection of Fig. 2c shows that, for the $n = 1$ LL, an increase in the correlation length causes only small modifications on the shape of this Landau band, plus an overall reduction of the width Γ_1 . Higher Landau levels, $n > 1$, show

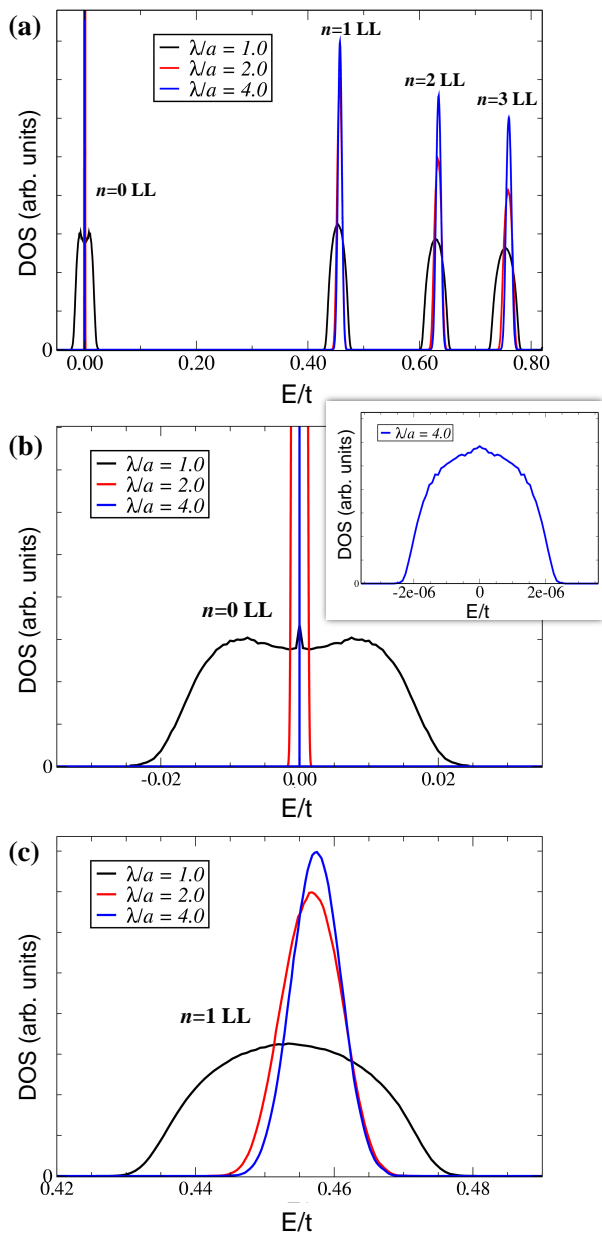


FIG. 2: (Color online) Density of states (in arbitrary units) for a magnetic flux $\Phi/\Phi_0=0.02$ for three different correlation lengths λ/a of the random hopping potential (in all cases $W/t = 0.3$ and the lattice size is $M \times N = 100 \times 90$ sites). (a) DOS showing the $n=0, 1, 2,$ and 3 Landau bands. (b) Zoom of the $n=0$ LL states. (c) Zoom of the $n=1$ LL states.

the same qualitative behavior as $n=1$. In contrast, for the $n=0$ LL (Fig. 2b), one observes a much stronger suppression of the level broadening upon increasing λ , in agreement with numerical results obtained in Ref. 25. However, the inset of Fig. 2b shows that, despite the large reduction of Γ_0 with increasing λ , the width never goes to zero within the range of λ we used. This is at odds with the results reported in Ref. 25, where an abrupt

transition to zero width was observed. It is worth mentioning that, when λ increases, making the width of the $n=0$ LL much smaller than the width of the higher levels, it is important to use DOS histograms with a much finer energy resolution around the $n=0$ LL than for the higher LLs. Not doing so can lead to an erroneous impression that the $n=0$ LL width vanishes sharply as the correlation length increases.

In the following, we describe how we define and quantify the width Γ_n of the disordered-broadened LLs. For the $n > 0$ LLs, which display a Gaussian-like shape, Γ_n is taken as the full width at half-height. Figure 2 clearly shows that the DOS shape of the $n=0$ LL is very different from the higher LLs. As pointed out in Ref. 24, an off-diagonal disorder model induces a splitting of the $n=0$ LL into two degeneracy-broken $n=0$ Landau bands, causing the observed DOS shape for the $n=0$ LL, namely, not fully split levels. This is so because the energy splitting always has the same order of magnitude of the LL broadening. Here, the $n=0$ LL shapes observed in Fig. 2b can be reasonably well fitted by a superposition of two equal Gaussian curves. Therefore, the $n=0$ LL width is considered as the width at half-height of one of these superposed bands (which is approximately half the width at half-height of the entire band).

Figure 3 shows how the LL widths decrease as the hopping disorder correlation length grows. In Fig. 3a, one observes that not only Γ_0 decreases with λ , but all other LLs do so. When examining the same data in a log-linear graph (Fig. 3b), one observes that the $n=0$ LL behaves quite differently from the others. For $n > 0$, the widths Γ_n decrease slowly with increasing λ/a . Figure 3 shows an apparent tendency to saturation at a value $\Gamma_n/t \approx 0.01$. We computed $\Gamma_{n>0}$ for larger values of λ/a (not shown here) and concluded that this is not quite correct. Instead, we observe that the rate by which all $\Gamma_{n>0}$ decrease becomes smaller as λ/a becomes larger. The behavior is very different for the $n=0$ LL, whose width decays exponentially with λ . This decay is sustained down to the numerical precision of our simulations.

Further insight about the effect of long-range correlated hopping disorder on the levels widths Γ_n can be gained from a perturbation theory analysis. Let us denote the disorder gauge potential by $V = H_{\pm} - H_0$, where both H and H_0 are defined in Sec. III.

In first order, the matrix elements required to calculate the energy corrections for the degenerate states that belong to the n th Landau level at the K valley are

$$V_{nK, k k'}^{(1)} = \langle \Psi_{n' k'}^K | V | \Psi_{nk}^K \rangle. \quad (10)$$

Since long-range hopping disorder does not mix valleys, K is a good quantum number in this model. As discussed in Sec. II, $E_0^{(1)} = 0$. For $n > 0$, the situation is different. Exact diagonalization in a $(n > 0, K)$ subspace involves matrix elements of the kind $V_{n \neq 0, K; k k'}^{(1)}$. Due to the spinor structure of Ψ_{nk}^K , the evaluation of such matrix elements amounts to the spatial integration of the

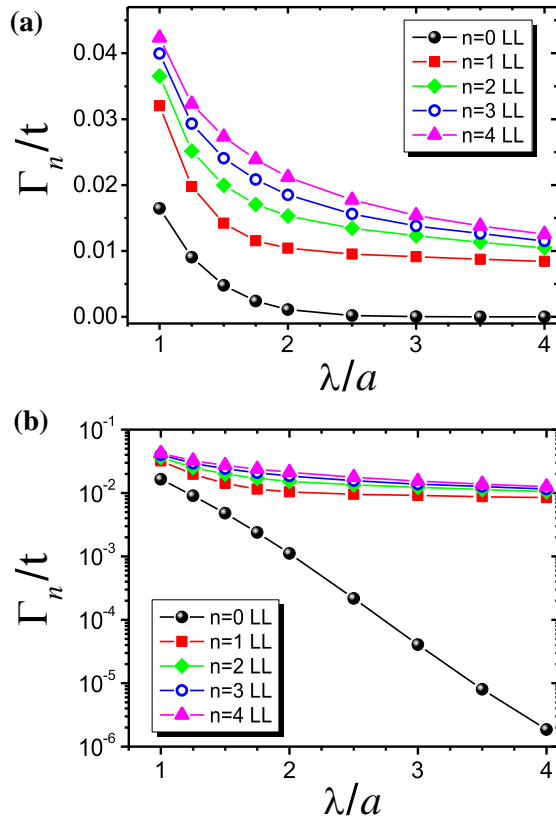


FIG. 3: (Color online) Width of the n th Landau level Γ_n/t , $n = 0, 1, 2, 3, 4$, as a function of the disorder correlation length λ/a for $\Phi/\Phi_0 = 0.02$ and $W/t = 0.3$. (a) Linear scale. (b) Log-linear scale.

product $\exp[i(k - k')y]\phi_{nk'}(x)\phi_{n-1,k}(x)$ times the Gaussian fluctuating gauge potential. This results in non-zero matrix elements, but they are very quickly suppressed as λ/ℓ_B becomes large.

Let us define

$$V_{nK,kk'}^{(2)} = \sum_{n' \neq n} \frac{|\langle \Psi_{n'k'}^K | V | \Psi_{nk}^K \rangle|^2}{\hbar\omega_B(\sqrt{n'} - \sqrt{n})} \quad (11)$$

to help us to discuss second-order effects. The evaluation of $V_{n=0,K;kk'}^{(2)}$ involves matrix elements where products of $\phi_{1,k'}$ and $\phi_{0,k}$ appear. For long-range disorder, such matrix elements vanish with increasing λ/ℓ_B . In summary, the perturbation fails to mix states within the $n = 0$ multiplet and also with $n' \neq 0$. Hence, we expect the same behavior at all order of perturbation theory. This is consistent with statement that $\Gamma_0 = 0$ for long-range hopping disorder.³⁰ Using the reasoning presented above, matrix elements of the kind $V_{n \neq 0,K;kk'}^{(2)}$ involve, among other components, the integration of products wave function amplitudes such as $\exp[i(k - k')y]\phi_{nk'}(x)\phi_{n,k}(x)$. These become small for $k \neq k'$ in the limit of $\lambda/\ell_B \gg 1$ and, for $k = k'$, are quite independent of $\lambda/\ell_B \gg 1$.

This analysis rules out long-range hopping disorder as the mechanism behind the exponential suppression of Γ_0

with increasing λ . We speculate that this behavior is caused by matrix elements that admix valleys, a remnant of the crossover regime. As a consequence, we expect Γ_0 to scale linearly with the disorder strength W and the eigenstates to be a superposition of a wave functions with probability amplitudes in both sublattices. Our simulations are in line with the latter statement, as we discuss below.

When a magnetic field is present, there is an important length scale to be considered, namely, the magnetic length; for convenience, let us write it in the form $\ell_B/a = 0.371/\sqrt{\Phi/\Phi_0}$. For the magnetic flux used in our simulations ($\Phi/\Phi_0 = 0.02$), we obtain $\ell_B/a = 2.62$, which is close to the values of λ/a used as well. Therefore, we expect the magnetic length to play a role in any interpretation of our results. Indeed, Fig. 3a suggests that the LL widths change its dependence with λ for $\lambda \gtrsim \ell_B$. However, Fig. 3b makes clear that a slow dependence on λ only occurs for the $n > 0$ LL. This is in line with our perturbative analysis. Unfortunately, the picture is not entirely consistent: We expect the second-order terms to be dominant in the calculation of the broadening of $\Gamma_{n>0}$ for λ/ℓ_B , which is not observed in the simulations (see discussion below). This remains to be understood.

We call attention to the fact that the authors of Ref. 25

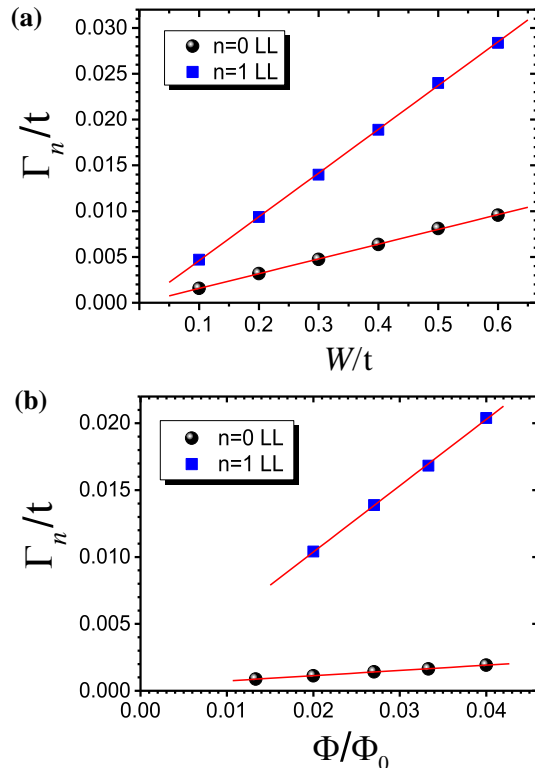


FIG. 4: (Color online) (a) Landau level width Γ_n/t as a function of the hopping disorder strength W/t for the $n=0$ and $n=1$ LLs (magnetic flux fixed at $\Phi/\Phi_0 = 0.02$ and $\lambda/a = 1.5$). (b) Γ_n as a function of magnetic flux Φ/Φ_0 for the same LLs (now for a fixed disorder strength $W/t = 0.3$ and $\lambda/a = 2.0$).

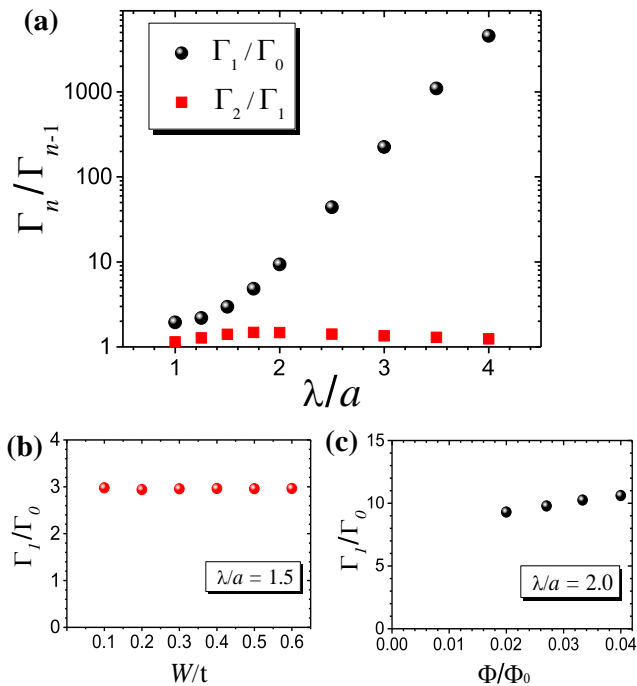


FIG. 5: (Color online) (a) Ratio between different Landau level widths Γ_n/Γ_{n-1} as a function of λ/a . The ratio between higher LLs widths, like Γ_2/Γ_1 , is quite independent of the correlation length λ . In contrast, the ratio Γ_1/Γ_0 grows rapidly with λ/a (notice the logarithmic scale). (b) Ratio Γ_1/Γ_0 as a function of the disorder strength W/t for $\lambda/a = 1.5$. (c) Ratio Γ_1/Γ_0 as a function of the magnetic flux Φ/Φ_0 for $\lambda/a = 2.0$. The panels (b) and (c) show that Γ_1/Γ_0 is almost independent of W/t and Φ/Φ_0 . In the log-linear plot of panel (a) the results corresponding to different values of W/t and Φ/Φ_0 collapse under the same dot.

used the same flux value we considered here, as well as a similar range for the correlation length λ . However, in our calculations, a finite width of the $n = 0$ LL can be seen even for $\lambda/a=4$ within the numerical precision we use. We checked (not shown here) that these results are not influenced by varying the system sizes, i.e., there are no finite lattice-size effects in the parameter region we investigated.

We have also investigated the dependence of the $n = 0$ and $n = 1$ LLs widths on the disorder and magnetic field amplitudes (Fig. 4). For both parameters, there is a clear linear increase.

Since the LL widths depend linearly on W and on Φ/Φ_0 , we conclude that there is universality in the behavior of the Landau level widths, namely, the ratio between different Landau level widths, $\Gamma_n/\Gamma_{n'}$, depends solely on λ/a . This is illustrated in Fig. 5a, where one can see the ratio Γ_1/Γ_0 growing rapidly with λ/a (notice the logarithmic scale), while Γ_2/Γ_1 remains essentially constant. This novel result allows our simulations to make contact with the experiments. Notice that due to computational limitations, our lattices sizes constrain us to consider unrealistically large values of magnetic field magnitudes.

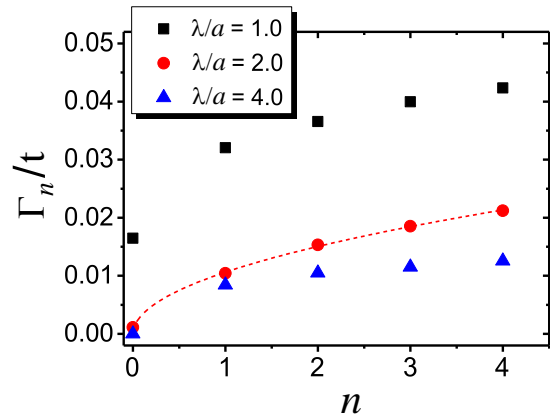


FIG. 6: (Color online) Landau level width Γ_n/t as a function of LL index n for three different values of λ/a , considering $\Phi/\Phi_0 = 0.02$ and $W/t = 0.3$ (same magnetic flux, disorder amplitude, and lattice sizes considered in Fig. 3). The dashed line corresponds to a fitting with square root dependence, which fits well only the $\lambda/a = 2$ case (see text).

However, since the ratios of LL widths are rather insensitive to the values of W and Φ/Φ_0 , as illustrated by Figs. 5b and c, we expect this result to apply for realistic settings as well.

The dependence of the width on the LL index is shown in Fig. 6. In this case as well, Γ_n increases with n when λ , W , and Φ are fixed (notice that the values for these parameters are the same considered in Fig. 3). We find that for $\lambda/a = 2$, the Γ_n versus n curve is perfectly fitted by the functional form $y = A\sqrt{x}$, with $A=0.0107$ (dashed line in Fig. 6). For other values of λ , including the cases $\lambda/a = 1$ and $\lambda/a = 4$, the numerical data do not show a square root dependence on LL index n . At this point, it is worth comparing these results to the effect of a diagonal disorder on the DOS in graphene at the quantum Hall regime. The Landau level broadening Γ_n for a diagonal white-noise disorder is quite independent of the LL index n ,^{22,23} while for the correlated diagonal disorder, Γ_n is observed to slightly decrease with increasing n .²² These effects for the diagonal disorder in graphene are similar to the observed for conventional quantum Hall systems with diagonal disorder models,³⁷ but are in clear contrast to the increase of Γ_n with n observed here.

V. LOCALIZATION PROPERTIES

While in Sec. IV we considered the DOS and analyzed the LL widths as a function of several parameters, we now investigate the localization properties of states within the LLs. To infer the degree of localization of the states we use the participation ratio (PR), which is defined as³⁸

$$\text{PR} = \frac{1}{N' \sum_{i=1}^{N'} |\psi_i|^4}, \quad (12)$$

where ψ_i is the amplitude of the normalized wave function on site i and $N' = M \times N$ is the total number of

lattice sites. The PR is therefore directly related to the proportion of the lattice sites over which the wave function is spread: the PR for a localized state vanishes in the thermodynamic limit, while peaks in the PR indicate the presence of extended states (critical energies).

Figure 7a shows the calculated PR in an energy window comprising the Landau levels $n=0, 1, 2,$ and 3 .

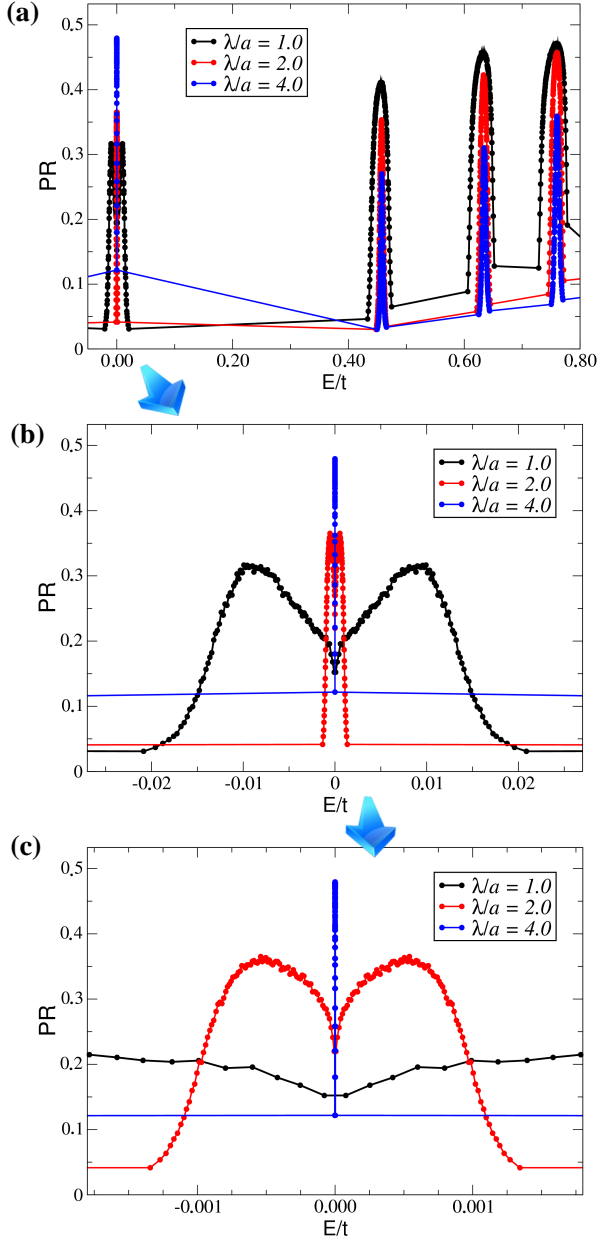


FIG. 7: (Color online) Participation Ratio as a function of E/t for different random hopping correlation lengths λ/a . Here, $\Phi/\Phi_0 = 0.02$, $W/t = 0.3$, and $M \times N = 100 \times 90$ (namely, the same magnetic flux, disorder amplitude, and lattice sizes considered in Fig. 3). (a) Energy window containing the four lowest LLs, $n=0, 1, 2,$ and 3 . (b) Zoom on the $n=0$ Landau level. (c) Amplified zoom on the $n=0$ states.

While the PR for the $n > 0$ LLs indicates the presence of localized states at Landau band tails and extended states at the band middle, as expected, the PR of the states from the $n=0$ LL shows a double hump structure, i.e., a splitting into two peaks. The splitting for the $n=0$ LL is more clearly observed in the energy scale zooms of Fig. 7b and c. The evidence that this double-peak structure in the PR of the $n=0$ LL corresponds to a splitting of critical energies is obtained through an analysis of the system-size dependence, as shown in Fig. 8. In this figure one observes how the PR for states within the $n=0$ and the $n=1$ LLs is modified with increasing system size, namely, for $M \times N = 100 \times 30, 100 \times 50,$ and 100×90 atoms in the disordered graphene lattice. For localized states, the PR decreases with increasing system size. This behavior is clearly seen at the Landau band tails and also in the region between the two peaks in Fig. 8a. In contrast, the PR peaks are almost independent of system size, provided the lattice dimensions exceed both the magnetic and correlation lengths, indicating that the states in these energy regions are extended (critical).³⁸

This splitting of critical energies in the lowest LL was

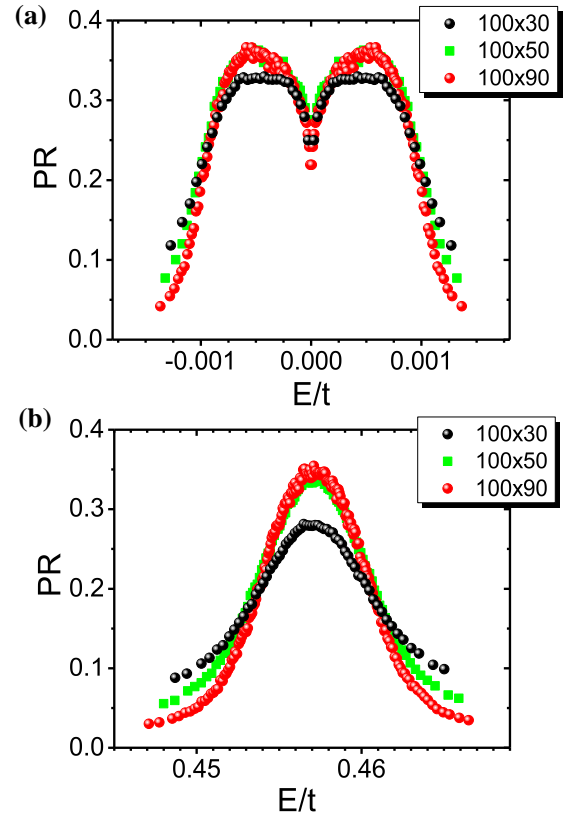


FIG. 8: (Color online) Participation ratio calculated for three different system-sizes ($M \times N$) for the states within (a) the $n=0$ LL and (b) the $n=1$ LL. The peaks identify the critical energies, as they become sharper when the system size increases. The results shown here are for a correlation length $\lambda/a=2.0$, and the other parameters are the same considered in Fig. 7: $\Phi/\Phi_0 = 0.02$ and $W/t = 0.3$.

previously observed and discussed for uncorrelated random hopping disorder^{21,24} (and for the similar case of uncorrelated random magnetic flux disorder^{31,32}). The novel and interesting aspect we observe here is that the splitting is rather robust and survives even the sharp width reduction of the $n=0$ LL due to the increasing correlation length. While previous works considered correlated random hopping disorder,^{25,26} they did not calculate the localization properties of the states within LLs and therefore missed this splitting of critical states at $n = 0$.

Although experiments⁹ have observed this splitting energy in the $n=0$ LL, it is hard to make a quantitative comparison due to the lattice size compromises we need to make in our simulations. Moreover, we believe that a full explanation of the experimentally observed splitting requires taking into account the Zeeman term and possibly electron-electron interactions, which calls for further theoretical investigation.

Due to particle-hole symmetry, the probability densities $|\Psi(E)|^2$ and the PR of states at energies $-E$ and $+E$ are identical (see, for instance, Ref. 16 and references therein). However, when looking directly at the wave function amplitudes $\Psi(E)$, one can see a difference between the split states at $-E$ and $+E$: In one of the sublattices (sublattice A , for example) the amplitudes are exactly the same, while in the other sublattice (B) they have the same magnitude but opposite signs, that is, $\Psi_A(-E) = \Psi_A(+E)$ and $\Psi_B(-E) = -\Psi_B(+E)$. This guarantees that conjugated particle-hole states are orthogonal and have the same probability densities $|\Psi(E)|^2$. It is noteworthy that orthogonality imposes that the probability weight at both sublattices is the same. The split states are therefore similar to bonding-antibonding states. The table in Fig. 9 summarizes these features.



n=0 LL state at energy = $-E$	n=0 LL state at energy = $+E$	
PR($-E$)	PR($+E$)	
$ \Psi(-E) ^2$	$ \Psi(+E) ^2$	
$\Psi(-E)$	$\Psi(+E)$	
$\Psi_A(-E)$	$\Psi_A(+E)$	→ sublattice A 
$\Psi_B(-E)$	$-\Psi_B(+E)$	→ sublattice B 

FIG. 9: (Color online) Properties of the wave functions Ψ for $n = 0$ LL states at energies $+E$ and $-E$. While the PR and the probability densities of the wave functions $|\Psi(E)|^2$ are identical for states at energies $-E$ and $+E$, the wave function amplitudes $\Psi(E)$ show differences in only one of the sublattices, in analogy to bonding-antibonding states (see text).

Another feature observed in Fig. 7 is the effect of increasing correlation length. The effect on the $n=0$ LL is completely different (opposite) to what is observed in higher levels. In higher levels, the increase in λ causes an overall reduction of PR values, while in the $n=0$ LL, despite the suppression of broadening (see Sec. IV), one observes an overall increase in the PR. This difference in behavior is probably related to the fact that the states from the higher levels have much longer localization lengths than those from the states with $n=0$.³⁷ To investigate possible finite-size effects on the $n = 0$ LL when λ/a is large, we ran simulations with larger lattice sizes (not shown). We found no change in the position of the identified critical states, as well as no change in the LL widths.

VI. CONCLUSIONS

We have investigated the effects of spatially correlated random hopping disorder on the structure of Landau levels in graphene. We quantified the behavior of the n th Landau level width Γ_n as a function of the correlation length, as well as other relevant parameters of the system: disorder amplitude, magnetic field, and Landau level index n . We found that Γ_n gets narrower with increasing correlation length for all Landau levels, and not only for the $n = 0$ level. However, a logarithmic plot of Γ_n as function of λ (Fig. 3b) clearly showed that while for $n > 0$ the widths decrease slowly, for $n = 0$ they decay exponentially with increasing λ . We found no sign of any abrupt vanishing of the $n = 0$ Landau level width at finite λ . This suggests that a different physical mechanism is behind the narrowing of the $n = 0$ LL when compared to all the other levels (specially when the correlation length λ becomes of the same order of magnitude or higher than the magnetic length ℓ_B). We speculate that the underlying mechanism is due to valley mixing, remnant of the crossover regime.

Γ_n increases linearly with both magnetic field and disorder amplitude. Another interesting observation is that for any fixed correlation length, Γ_n always increases with increasing LL index n , which is completely different to the dependence observed for diagonal (on-site) disorder models. More importantly, we observe that the ratio between the $n=1$ and $n=0$ Landau level widths, Γ_1/Γ_0 , depends only on the correlation length λ and is rather insensitive to the disorder strength and to the magnitude of the applied magnetic field. This allows a closer contact of our results with experiments. In Ref. 11, for instance, the authors experimentally observe a $n = 0$ LL width of about 20K, while the width of higher levels is observed to be about 400K, resulting in $\Gamma_1/\Gamma_0 = 20$. Using this information and the results of our Fig. 5, we infer that $\lambda/a = 2.2$. This estimate gives a lower bound for the corrugation length of graphene in the experiment of Ref. 11, since it neglects all disorder broadening sources but hopping disorder.

We also considered the role played by changing the

hopping disorder correlation length on the localization properties of the states within the different Landau levels. The splitting of two critical energies for the $n = 0$ level, previously reported for uncorrelated random hoppings,²⁴ is still clearly defined for correlated hopping disorder. It is a robust effect even with the sharp width reduction of the $n = 0$ level that occurs for large values of λ . The $n = 0$ level can therefore be considered as a superposition of two levels with broken degeneracy, symmetrically split around $E = 0$. In addition, after analyzing the wave functions of states belonging to the $n = 0$ level, we were able to identify a symmetric structure of these states. We found that although any two states at $-E$ and $+E$ have the same probability density and also the same participation ratio, in one sublattice the wave function amplitudes of states with energies $\pm E$ are exactly the same, while in the other sublattice these states have the same magnitude but opposite signs. Therefore, the origin for this $n = 0$ level splitting is clearly related to the breaking of the sublattice degeneracy induced by the hopping disorder, a further manifestation of the influence of valley mixing disorder.

Acknowledgments

This work has been supported by the Brazilian funding agencies FAPERJ, FAPESP, and CNPq. E.R.M. acknowledges partial financial support from the NSF award DMR 1006230. Simulations were performed at the computational facilities of LACAD-UERJ and CENAPAD-SP. The authors thank P. A. Schulz for his suggestions and critical reading of the manuscript.

-
- ¹ K. S. Novoselov, A. K. Geim, S. V. Morozov, D. Jiang, M. I. Katsnelson, I. V. Grigorieva, S. V. Dubonos, and A. A. Firsov, *Nature* **438**, 197 (2005).
- ² Y. Zhang, Y. W. Tan, H. L. Stormer, and P. Kim, *Nature* **438**, 201 (2005).
- ³ K. S. Novoselov, Z. Jiang, Y. Zhang, S. V. Morozov, H. L. Stormer, U. Zeitler, J. C. Maan, G. S. Boebinger, P. Kim, and A. K. Geim, *Science* **315**, 1379 (2007).
- ⁴ M. L. Sadowski, G. Martinez, M. Potemski, C. Berger, and W. A. de Heer, *Phys. Rev. Lett.* **97**, 266405 (2006).
- ⁵ R. S. Deacon, K.-C. Chuang, R. J. Nicholas, K. S. Novoselov, and A. K. Geim, *Phys. Rev. B* **76**, 081406 (2007).
- ⁶ Z. Jiang, E. A. Henriksen, L. C. Tung, Y.-J. Wang, M. E. Schwartz, M. Y. Han, P. Kim, and H. L. Stormer, *Phys. Rev. Lett.* **98**, 197403 (2007).
- ⁷ D. L. Miller, K. D. Kubista, G. M. Rutter, M. Ruan, W. A. de Heer, P. N. First, and J. A. Stroscio, *Science* **324**, 924 (2009).
- ⁸ G. Li, A. Luican, and E. Y. Andrei, *Phys. Rev. Lett.* **102**, 176804 (2009).
- ⁹ Z. Jiang, Y. Zhang, H. L. Stormer, and P. Kim, *Phys. Rev. Lett.* **99**, 106802 (2007).
- ¹⁰ A. J. M. Giesbers, U. Zeitler, M. I. Katsnelson, L. A. Ponomarenko, T. M. Mohiuddin, and J. C. Maan, *Phys. Rev. Lett.* **99**, 206803 (2007).
- ¹¹ A. J. M. Giesbers, L. A. Ponomarenko, K. S. Novoselov, A. K. Geim, M. I. Katsnelson, J. C. Maan, and U. Zeitler, *Phys. Rev. B* **80**, 201403R (2009).
- ¹² A. J. M. Giesbers, U. Zeitler, L. A. Ponomarenko, R. Yang, K. S. Novoselov, A. K. Geim, and J. C. Maan, *Phys. Rev. B* **80**, 241411R (2009).
- ¹³ U. Zeitler, A. J. M. Giesbers, A. McCollam, E. V. Kurganova, H. J. van Elferen, and J. C. Maan, *J. Low Temp Phys.* **159**, 238 (2010).
- ¹⁴ A. H. Castro Neto, F. Guinea, N. M. R. Peres, and K. S. Novoselov, *Rev. Mod. Phys.* **81**, 109 (2009).
- ¹⁵ E. R. Mucciolo and C. H. Lewenkopf, *J. Phys.: Cond. Mat.* **22**, 273201 (2010).
- ¹⁶ D. Abergel, V. Apalkov, J. Berashevich, K. Ziegler, and T. Chakraborty, *Adv. Phys.* **59**, 261 (2010).
- ¹⁷ S. Das Sarma, S. Adam, E. H. Hwang, and E. Rossi, *Rev. Mod. Phys.* **83**, 407 (2011).
- ¹⁸ J. Martin, N. Akerman, G. Ulbricht, T. Lohmann, K. von Klitzing, J. H. Smet, and A. Yacoby, *Nature Phys.* **5**, 669 (2009).
- ¹⁹ F. Guinea, M. I. Katsnelson, and M. A. H. Vozmediano, *Phys. Rev. B* **77**, 075422 (2008).
- ²⁰ M. A. H. Vozmediano, M. I. Katsnelson, and F. Guinea, *Phys. Rep.* **496**, 109 (2010).
- ²¹ M. Koshino and T. Ando, *Phys. Rev. B* **75**, 033412 (2007).
- ²² A. L. C. Pereira and P. A. Schulz, *Phys. Rev. B* **77**, 075416 (2008).
- ²³ W. Zhu, Q. W. Shi, X. R. Wang, J. Chen, J. L. Yang, and J. G. Hou, *Phys. Rev. Lett.* **102**, 056803 (2009).
- ²⁴ A. L. C. Pereira, *New J. Phys.* **11**, 095019 (2009).
- ²⁵ T. Kawarabayashi, Y. Hatsugai, and H. Aoki, *Phys. Rev. Lett.* **103**, 156804 (2009).
- ²⁶ T. Kawarabayashi, Y. Hatsugai, and H. Aoki, *Physica E* **42**, 759 (2010).
- ²⁷ W. Zhu, Q. W. Shi, J. G. Hou, and X. R. Wang, *arXiv:1006.0545* (2010).
- ²⁸ C. H. Yang, F. M. Peeters, and W. Xu, *Phys. Rev. B* **82**, 075401 (2010).
- ²⁹ C. H. Yang, F. M. Peeters, and W. Xu, *Phys. Rev. B* **82**, 205428 (2010).
- ³⁰ P. M. Ostrovsky, I. V. Gornyi, and A. D. Mirlin, *Phys. Rev. B* **77**, 195430 (2008).
- ³¹ L. Schweitzer and P. Markoš, *Phys. Rev. B* **78**, 205419 (2008).
- ³² L. Schweitzer, *Phys. Rev. B* **80**, 245430 (2009).
- ³³ K. Wakabayashi, M. Fujita, H. Ajiki, and M. Sigrist, *Phys. Rev. B* **59**, 8271 (1999).
- ³⁴ N. H. Shon and T. Ando, *J. Phys. Soc. Japan* **67**, 2421 (1998).
- ³⁵ Y. Zheng and T. Ando, *Phys. Rev. B* **65**, 245420 (2002).
- ³⁶ D. A. Abanin, P. A. Lee, and L. S. Levitov, *Phys. Rev. Lett.* **98**, 156801 (2007).
- ³⁷ T. Ando and Y. Uemura, *J. Phys. Soc. Japan* **36**, 959 (1974).
- ³⁸ D. J. Thouless, *Phys. Rep.* **13**, 93 (1974).